PHYSICAL REVIEW B **89**, 180405(R) (2014)

Observation of Bloch-point domain walls in cylindrical magnetic nanowires

S. Da Col,[1,2] S. Jamet,[1,2] N. Rougemaille,[1,2] A. Locatelli,[3] T. O. Mentes,[3] B. Santos Burgos,[3] R. Afid,[1,2] M. Darques,[1,2,*] L. Cagnon,[1,2] J. C. Toussaint,[1,2] and O. Fruchart[1,2,†]

[1]*Université Grenoble Alpes, Inst NEEL, F-38042 Grenoble, France*

[2]*CNRS, Inst NEEL, F-38042 Grenoble, France*

[3]*Elettra - Sincrotrone Trieste S.C.p.A., I-34012 Basovizza, Trieste, Italy*

(Received 1 December 2013; revised manuscript received 23 April 2014; published 12 May 2014)

Topological protection is an efficient way of warranting the integrity of quantum and nanosized systems. In magnetism, one example is the Bloch point, a peculiar three-dimensional object implying the local vanishing of magnetization within a ferromagnet. By combining surface and transmission x-ray magnetic circular dichroism photoemission electron microscopy, we experimentally confirm the existence of the simplest magnetization texture holding a Bloch point at rest: the Bloch-point domain wall in cylindrical magnetic nanowires. This opens the way to the experimental search for peculiar phenomena predicted during the motion of these protected Bloch-point-based domain walls.

DOI: 10.1103/PhysRevB.89.180405 PACS number(s): 75.60.Ch, 68.37.Xy, 75.70.Kw, 75.75.Fk

There is increasing attention towards physical systems providing topological protection. The interest is both fundamental, to elucidate the underlying physical phenomena, and applied, as a means to provide robustness to a state against external perturbations and decoherence. For example, the peculiar topology of the band structure of carbon nanotubes and graphene forbids backscattering of charge carriers [1], an effect which is often invoked to explain the high mobilities up to room temperature [2]. A similar effect occurs at the surface of so-called topological insulators, together with a locking of the spin of charge carriers; this provides spin currents protected against depolarization [3]. A photonic analog has also been designed by combining helical waveguides on a lattice with a graphenelike honeycomb topology, removing time-reversal symmetry and thereby preventing backscattering of light [4].

In systems displaying a directional order parameter such as liquid crystals and ferromagnets, interesting phenomena are associated with the slowly varying texture of the order field (magnetization for a ferromagnet). The requirement of local continuity of a vector field with fixed magnitude provides a topological protection against an arbitrary transformation of the texture. A prototypical case in magnetism is skyrmions, which are essentially local two-dimensional chiral spin textures stabilized by the Dzyaloshinskii-Moriya interaction, embedded in an otherwise uniformly magnetized surrounding. Despite these surroundings, skyrmions cannot unwind continuously as explained by the above continuity constraints of the magnetization field, explaining their topological protection. Skyrmions were first predicted theoretically [5], then confirmed experimentally in both bulk [6] and thin-film forms [7].

Bloch points are yet another type of topologically protected magnetic texture which cannot be unwound, but are of a three-dimensional nature. Bloch points are such that given the distribution of magnetization set on a closed surface such as a sphere, the enclosed volume cannot be mapped with a continuous magnetization field of finite magnitude. This occurs, e.g., for hedgehog configurations or, more generally, whenever all directions of magnetization are mapped on the closed surface [Figs. 1(a) and 1(b)]. Such boundary conditions imply the local cancellation of the modulus of magnetization on at least one location, which is a singularity for a ferromagnetic material. Although of finite, however close-to-atomic, size because of the cost in exchange energy, the Bloch point is topologically protected by its extended boundary conditions. Bloch points were predicted theoretically [8,9], their existence being suspected from the examination of extended boundary conditions at the surfaces of three-dimensional samples such as former bubble-memory media [10].

The interest in Bloch points was revived in recent years. As zero-dimensional objects, they were predicted to be required in the transient state allowing magnetization reversal along one-dimensional objects, such as magnetic vortices [11]. Due to their atomic size, Bloch points are thought to be subject to pinning at atomic sites on the underlying crystal [11–13]. Based on the interaction with these pinning sites, it was postulated that a moving Bloch point emits THz waves. Bloch points have also been predicted to exist at rest in magnetic nanowires with a compact cross section such as a cylindrical one. In nanowires, two types of domain walls (DWs) have indeed been predicted to exist: the transverse wall (TW) and the Bloch-point wall (BPW) [14,15] [Figs. 1(c) and 1(d)]. The former is topologically equivalent to the transverse and vortex walls in flat strips [Figs. 1(e) and 1(f)], in which a flux of induction runs across the structure. To the contrary, the latter has a distinct topology: magnetization remains locally mostly parallel to the surface at any location, allowing a decrease of the magnetostatic energy. In other words, no flux line flows across the wire. As described above, these boundary conditions impose the existence of a Bloch point, which is predicted to sit on the axis of the wire. The DW of lowest energy should be the TW for wires diameter smaller than roughly seven times the dipolar exchange length $\Delta_d = \sqrt{2A/\mu_0 M_s^2}$, while the BPW should be the ground state for larger diameters. Nevertheless, each type of DW should exist as a metastable state over a significant range of diameters.

While there is no doubt about the relevance of Bloch points, although their direct imaging remains a challenge, so far hints for static Bloch points were reported only in

*Now at: Nexans research center, 69007 Lyon, France.

†Olivier.Fruchart@neel.cnrs.fr

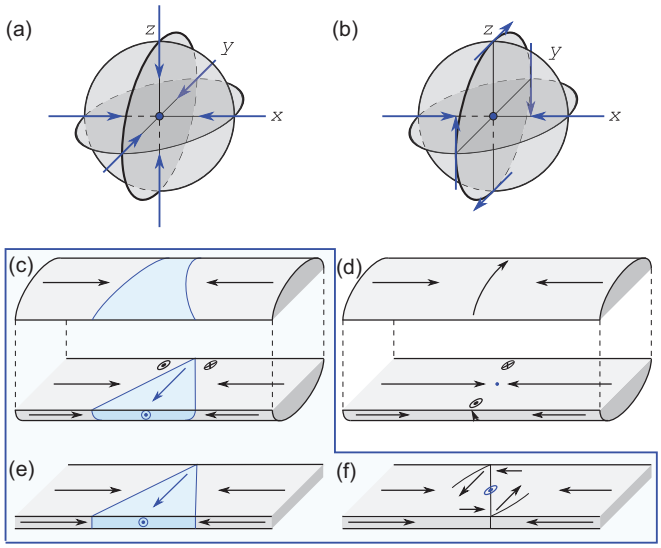

FIG. 1. (Color online) Sketches for magnetization textures. (a),(b) Two of the various possible textures of magnetization around a Bloch point. (b) is obtained from (a) with a quarter turn of magnetization around the x axis. (c),(d) Cylindrical wires with DWs of the transverse and Bloch-point type, respectively. (e),(f) Strips with in-plane magnetization with DWs of the transverse and vortex type, respectively. Notice the identical boundary conditions around the Bloch point in (b) and (d). (c),(e),(f) DWs share the same topology, characterized by a volume of induction going through the system along a transverse direction, depicted in blue. The Bloch-point DW is of a different class and cannot be mapped continuously to the wire TW.

extended systems. However, the large number of degrees of freedom in such systems makes it very difficult to investigate the physics specifically related to the Bloch point and their topological protection, especially during magnetization dynamics. The interest in BPWs is that they are the simplest magnetization texture holding a Bloch point, with specific physical consequences. For instance, micromagnetic simulation predicts that the topological protection of the BPW prevents its transformation into other types of DWs during its motion [14,15]. As a consequence, DW speeds beyond 1 km/s should be reachable, opening the way to new physics such as the spin-Cherenkov effect through interaction of the DW with standing spin waves [16]. This is in strong contrast with the more common case of flat strips made by lithography, for which the two possible DWs share a common topology, so that periodic transformation from one to another during DW motion severely limits the average mobility, and motion is nonstationary [15,17]. The emission of THz waves resulting from the interaction with the lattice should also be easier to evidence in such one-dimensional (1D) tracks, compared to extended systems.

The existence of BPWs has not been experimentally confirmed yet. Here we report on the use of a three-dimensional high-spatial-resolution magnetic imaging technique to gather both surface and volume information of the magnetization texture of DWs in cylindrical nanowires, and formally identify the BPW. These results are supported by the development of a postprocessing code of three-dimensional magnetization textures to analyze the experimental magnetic contrast.

We first prepared self-organized anodized alumina templates in 0.3 M oxalic acid at either 40 or 135 V, yielding pore diameters of 35 and 120 nm, respectively [18]. For some templates, we modulated the voltage from 135 to 150 V so as to vary the diameter of pores along their length [19]. We also made use of atomic layer deposition to uniformly reduce the diameter along their length. We then electroplated $Fe_{20}Ni_{80}$ (permalloy) micrometers-long nanowires in these. The filled alumina templates were dissolved in a NaOH solution, followed by several rinsing steps in water and finally in isopropyl alcohol. Drops of solution were deposited on doped Si wafers. To identify the nature of the DWs, we applied element-sensitive x-ray magnetic circular dichroism photoemission electron microscopy (XMCD-PEEM), carried out using the setup [20] operating at the undulator beam line Nanospectroscopy at Elettra, Sincrotrone Trieste. The photons impinge on the supporting surface with a grazing angle of 16°. In this Rapid Communication, we present data based on secondary photoelectron emission at the Fe L_3 edge using essentially circularly polarized radiation as a probe. The XMCD magnetic contrast was obtained by the difference of images with opposite helicities σ_+ and σ_- of the photon beam, normalized to their sum XPEEM: $I_{\mathrm{XMCD}} = (I_{\sigma_-} - I_{\sigma_+})/(I_{\sigma_-} + I_{\sigma_+})$. By convention, positive contrast means magnetization parallel to the photon beam. The spatial resolution in XMCD-PEEM is ≈30 nm. Micromagnetic simulations were performed using FEELLGOOD, a home-built code based on the temporal integration of the Landau-Lifshitz-Gilbert equation in a finite-element scheme, i.e., using tetrahedra to discretize the nanowires [21]. Only exchange and magnetostatic interactions were taken into account to deal with the present case of magnetically soft wires. The parameters for bulk permalloy were used: $A = 10^{-11}$ J/m and $\mu_0 M_s = 1$ T, for which $\Delta_d \approx 5$ nm. The tetrahedron size was about 4 nm.

Whereas magnetic nanowires gave rise to numerous experimental reports [22], essentially macroscopic and full magnetization reversal was probed [23]. One reason is that magnetization is constrained to remain essentially along the wire due to magnetostatics. Magnetization switching thus proceeds under a significant applied magnetic field through nucleation of a DW at one end, followed by its fast motion towards its other end, leading to its annihilation. To stabilize DWs in nanowires, we make use of local protrusions placed several micrometers apart to act as potential barriers against DW motion. While these barriers are not sufficient to pin DWs when a large magnetic field is applied along the wire to force nucleation [24], we found that they are fit to prevent motion of DWs upon dc oscillatory demagnetization with the magnetic field applied perpendicular to the wafer plane.

The type of DWs thus created was examined by XMCD-PEEM. Thanks to the three-dimensional nature of nanowires, we could collect both direct photoemission, as usually done, and also transmission data, as shown on Fig. 2. Direct photoemission provides magnetic contrast on the wires. As the secondary electrons collected by the microscope have a mean free path of a few nanometers only, this contrast informs us of surface magnetization only. We also analyzed the magnetic contrast formed in the shadow by the light

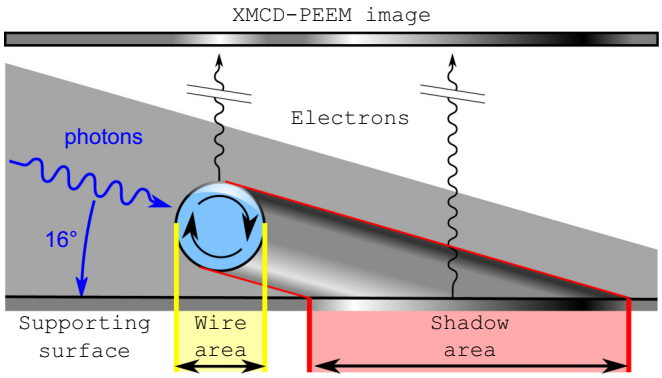

FIG. 2. (Color online) Schematic of the principle of the dual surface transmission-projection PEEM, with magnetic sensitivity based on XMCD. The gray level stands for the dichroic signal (normalized difference with photons of opposite helicity).

partially transmitted through the wire [25]. This allows us to gain information about the magnetization arrangement in the bulk of the wires, integrated along the path of light. Gathering this information is crucial, as identification of the DW type may otherwise be ambiguous if relying solely on the map of surface magnetization. Besides, this allows us to check the arrangement of magnetization in the vicinity of the wire axis, where Bloch points are expected. Finally, notice that thanks to the rather grazing incidence $\alpha = 16°$, the shadow is inflated with respect to the wire diameter by a factor of $1/\sin\alpha \approx 3.6$, thereby potentially bringing the spatial resolution of the microscope in this projection mode to around 10 nm.

In a first step, the wires are aligned along the photon beam so as to identify longitudinal domains, and thus highlight the location of DWs. In a second step, the sample is rotated by 90° so that the wires are aligned in the direction transverse to the photon beam. Under this configuration, contrast solely arises from DWs [Figs. 3(a) and 3(b)]. We observed two well-defined families of DWs, typical examples being shown in Figs. 3(c) and 3(d). The first family is characterized by an orthoradial curling of magnetization as identified from the shadow, and it is symmetric with respect to a plane perpendicular to the wire axis. Notice the absence of contrast on the axis, as expected for the presence of a BP. The second type of DW breaks the above-mentioned symmetry, and is now characterized by a monopolar contrast at the center of the DW, in the vicinity of the wire axis. This is expected for TWs, the contrast on the axis arising from the transverse component of magnetization with respect to the beam. Consistent with predictions [15] and based on a dozen observations, DWs in wires with a large diameter were always found of the type ascribed to BPWs, while those for smaller diameter were always found of the TW type, with a crossover diameter in the range 70–90 nm.

We developed simulations to allow for a quantitative analysis of the experimental contrasts and strengthen the symmetry arguments provided above. Starting from crude micromagnetic distributions similar to the two depicted in Figs. 1(c) and 1(d), the system is allowed to evolve and dissipate energy to finally reach a local minimum in either the TW or BPW state [Figs. 3(e) and 3(f)]. These configurations

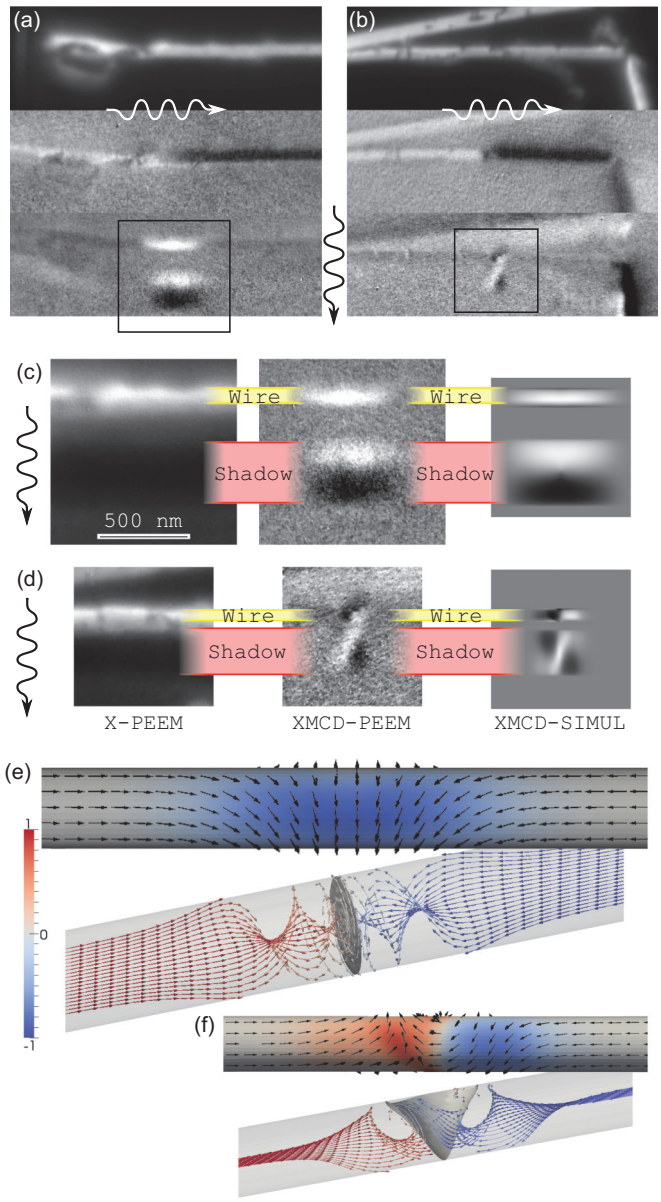

FIG. 3. (Color online) Identification of the Bloch-point and transverse domain walls based on XMCD-PEEM compared with simulations. (a),(b) In each are three views of the same wire, at the same location and with a field of view 3×1 μm. From top to bottom: total absorption and XMCD contrast parallel and across the wires. (c),(d) From left to right: X-PEEM (sum of images for the two polarizations), XMCD-PEEM [enlargement of the square areas in (a) and (b)], and simulations of two DWs at the Fe L3 edge. The photons arrive from the upper part of the images. (c) A wire of diameter 95 nm lifted 80 nm above the surface, with a DW identified of the Bloch-point type. (d) A wire of diameter 70 nm lifted 25 nm above the surface, with a DW identified of the transverse type. (e),(f) Top view and open view of the micromagnetic state used in the right parts of (c) and (d), with wire diameter 95 and 70 nm, respectively.

are then postprocessed to deliver a simulation of XMCD-PEEM contrast. To do this, the wire is intercepted with a dense beam of parallel lines, each acting as the trace of a photon. First, for each photon helicity, the probabilistic absorption of every trace is integrated along its path through

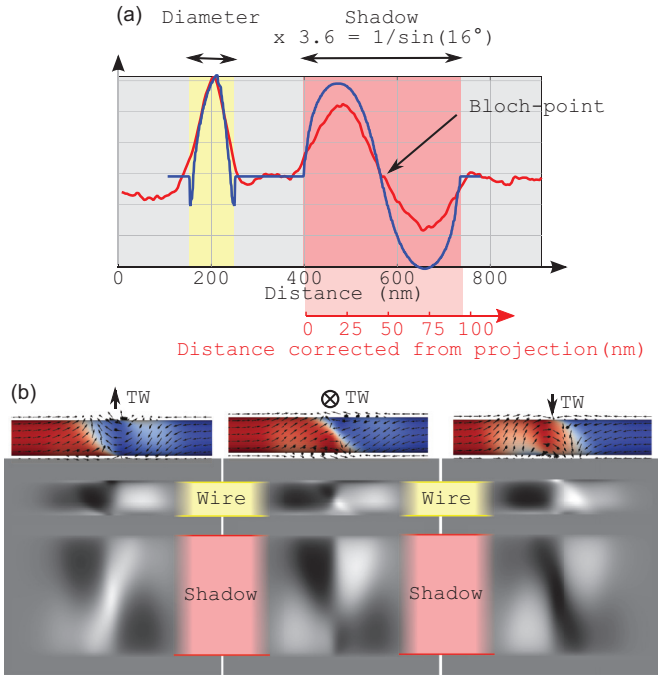

FIG. 4. (Color online) (a) Comparison of the experimental and simulated cross section of the contrast of a Bloch-point domain wall along the direction transverse to the wire. Data from 3(c). (b) Contrast arising from a transverse wall with various azimuth. The wire is 70 nm in diameter and lifted 25 nm above the surface.

the nanowire. The absorption coefficient per unit length is calculated depending on the local direction of magnetization with respect to the propagation vector, and is different for the two photon helicities. Second, the photoemission process is simulated. Given the small mean free path of the low-energy electrons collected in the microscope, we considered only those electrons emitted at the very surface, proportionally to the local absorption. At the surface of the magnetic wire, we computed I_{σ_-} and I_{σ_+} as the intensity of each beam helicity multiplied by the magnetization-dependent absorption, for both incoming and outgoing photons. However, at the surface of the nonmagnetic supporting surface where the shadow is projected, the difference signal only reflects the imbalance of the photon intensities.

The simulations reproduce all features of the experimental contrast. The agreement of simulations with experiments is quantitative; see, for example, the rapid increase of width of the DW with the diameter of the nanowire [Fig. 3(c) versus 3(d)] or the exact shape across the BPW [Fig. 4(a)] with zero contrast at the expected location of the Bloch point. Concerning the latter, the experimental contrast is smaller than expected in the shadow due to the existence of a uniform background of scattered electrons impinging on the camera, decreasing the XMCD contrast to a larger extent where the number of direct electrons is smaller. As regards the TW, the black and white features at the surface of the wire are shown to result from the curling of magnetization around the transverse core. Different azimuths of the core of the TW yield different contrasts, but none with a mirror symmetry and thus unmistakably different from the contrast expected for a BPW [Fig. 4(b)]. As over the past ten years simulations in nanowires yielded DWs of no other types than TW or BPW, this shows that what we have unambiguously imaged are BPWs. Note, finally, that even though we do not directly image the Bloch point, expected to be the size of about one nanometer, note that, in contrast to previous report, here the local environment of a Bloch point is imaged with bulk information and spatial resolution of the order of the relevant micromagnetic characteristic length scale, i.e., the dipolar exchange length. Thus there can be no micromagnetic magnetization texture left unresolved in our experiments.

The experimental demonstration of the existence of BPWs opens the way for the investigation of its peculiar behavior of motion, predicted numerically. We mentioned its expected steady motion and high velocity [15]. It is with this prospect that we used permalloy as a material, to avoid local anisotropy and magnetostriction. While those are not expected to have an impact on the DW structure itself due to the large magnetostatic energy determining its structure, they may induce the pinning of DWs by creating an irregular landscape of energy along the wire [26]. To check this, we have investigated the response of both types of DWs to quasistatic pulses of magnetic field, inspecting the DWs with magnetic force microscopy. The propagation field remains moderate, in the range 1–10 mT. This is comparable to, e.g., that of perpendicularly magnetized strips, where DW motion could be extensively investigated [27,28]. These wires should therefore be already suitable to confirm the predictions for the motion of BPWs [15,29], while progress in material control is expected after this demonstration. Besides fundamental studies, this should also redraw attention to the proposal of a three-dimensional race-track memory based on 2D arrays of parallel cylindrical nanowires [30,31].

The research leading to these results has received funding from the European Unions's 7th Framework Programme under grant agreement No. 309589 (M3d). We gratefully acknowledge the help of E. Wagner for the demagnetization of samples, Ph. David for the preparation of MFM tips, Simon Le Denmat for technical support with AFM/MFM, and fruitful discussions with J. Vogel, S. Pizzini, J. Coraux, and M. Staño.

[1] T. Ando, T. Nakanishi, and R. Saito, J. Phys. Soc. Jpn. **67**, 2857 (1998).

[2] K. S. Novoselov, Z. J. Y. Zhang, S. V. Morozov, H. L. Stormer, U. Zeitler, J. C. Maan, G. S. Boebinger, P. Kim, and A. K. Geim, Science **315**, 1379 (2007).

[3] M. König, S. Wiedmann, C. Brüne, A. Roth, H. Buhmann, L. W. Molenkamp, X.-L. Qi, and S.-C. Zhang, Science **318**, 766 (2007).

[4] M. C. Rechtsman, J. M. Zeuner, Y. Plotnik, Y. Lumer, D. Podolsky, F. Dreisow, S. Nolte, M. Segev, and A. Szameit, Nature (London) **496**, 196 (2013).

[5] A. N. Bogdanov and D. A. Yablonskii, Sov. Phys. JETP **68**, 101 (1989).
[6] X. Z. Yu, Y. Onose, N. Kanazawa, J. H. Park, J. H. Han, Y. Matsui, N. Nagaosa, and Y. Tokura, Nature (London) **465**, 901 (2010).
[7] N. Romming, C. Hanneken, M. Menzel, J. E. Bickel, B. Wolter, K. von Bergmann, A. Kubetzka, and R. Wiesendanger, Science **341**, 636 (2013).
[8] R. Feldkeller, Z. Angew. Physik **19**, 530 (1965).
[9] W. Döring, J. Appl. Phys. **39**, 1006 (1968).
[10] A. P. Malozemoff and J. C. Slonczewski, *Magnetic Domain Walls in Bubble Materials* (Academic, New York, 1979).
[11] A. Thiaville, J. M. García, R. Dittrich, J. Miltat, and T. Schrefl, Phys. Rev. B **67**, 094410 (2003).
[12] S. K. Kim and O. Tchernyshyov, Phys. Rev. B **88**, 174402 (2013).
[13] H.-G. Piao, J.-H. Shim, D. Djuhana, and D.-H. Kim, Appl. Phys. Lett. **102**, 112405 (2013).
[14] H. Forster, T. Schrefl, D. Suess, W. Scholz, V. Tsiantos, R. Dittrich, and J. Fidler, J. Appl. Phys. **91**, 6914 (2002).
[15] A. Thiaville and Y. Nakatani, *Spin Dynamics in Confined Magnetic Structures III* (Springer, Berlin, 2006), Vol. 101, pp. 161–206.
[16] M. Yan, C. Andreas, A. Kakay, F. Garcia-Sanchez, and R. Hertel, Appl. Phys. Lett. **99**, 122505 (2011).
[17] A. Thiaville and Y. Nakatani, *Nanomagnetism and Spintronics* (Elsevier, New York, 2009).
[18] W. Lee, R. Ji, U. Gösele, and K. Nielsch, Nat. Mater. **5**, 741 (2006).
[19] W. Lee, K. Schwirn, M. Steinhart, E. Pippel, R. Scholz, and U. Gösele, Nat. Naotech. **3**, 234 (2008).
[20] A. Locatelli, L. Aballe, T. O. Menteş, M. Kiskinova, and E. Bauer, Surf. Interface Anal. **38**, 1554 (2006).
[21] F. Alouges, E. Kritsikis, and J.-C. Toussaint, Physica B **407**, 1345 (2012).
[22] A. Fert and J. L. Piraux, J. Magn. Magn. Mater. **200**, 338 (1999).
[23] T. Wang, Y. Wang, Y. Fu, T. Hasegawa, F. S. Li, H. Saito, and S. Ishio, Nanotechnology **20**, 105707 (2009).
[24] K. Pitzschel, J. Bachmann, S. Martens, J. M. Montero-Moreno, J. Kimling, G. Meier, J. Escrig, K. Nielsch, and D. Görlitz, J. Appl. Phys. **109**, 033907 (2011).
[25] J. Kimling, F. Kronast, S. Martens, T. Böhnert, M. Martens, J. Herrero-Albillos, L. Tati-Bismaths, U. Merkt, K. Nielsch, and G. Meier, Phys. Rev. B **84**, 174406 (2011).
[26] A. A. Ivanov and V. A. Orlov, Phys. Solid State **53**, 12 (2011).
[27] T. A. Moore, M. Miron, G. Gaudin, G. Serret, S. A. B. Rodmacq, A. Schuhl, S. Pizzini, J. Vogel, and M. Bonfim, Appl. Phys. Lett. **93**, 262504 (2008).
[28] I. M. Miron, T. Moore, H. Szambolics, L. D. Buda-Prejbeanu, S. Auffret, B. Rodmacq, S. Pizzini, J. Vogel, M. Bonfim, A. Schuhl, and G. Gaudin, Nat. Mater. **10**, 419 (2011).
[29] M. Yan, A. Kákay, S. Gliga, and R. Hertel, Phys. Rev. Lett. **104**, 057201 (2010).
[30] S. S. P. Parkin, U.S. Patents No. 6834005, No. 6898132, and No. 6920062 (2003).
[31] S. S. P. Parkin, M. Hayashi, and L. Thomas, Science **320**, 190 (2008).